Research Article | Vol. 10, No. 3 | 1 Mar 2019 | BIOMEDICAL OPTICS EXPRESS 1184
Biomedical Optics EXPRESS

In vivo monitoring and high-resolution characterizing of the prednisolone-induced osteoporotic process on adult zebrafish by optical coherence tomography

YANPING LIN,[1] XIANG XIANG,[1] TINGRU CHEN,[1] CHUDAN GAO,[1] HONGBO FU,[1] LIMEI WANG,[2] LIJUN DENG,[3] LVMING ZENG,[3,4] AND JIAN ZHANG[1,*]

[1]*School of Basic Medical Science, Affiliated Stomatology Hospital of Guangzhou Medical University, Guangzhou Medical University, Guangzhou 511436, China*
[2]*Center for Drug Non-clinical Evaluation and Research, Guangdong Biological Resources Institute, Guangdong Academy of Sciences, Guangzhou 510900, China*
[3]*Key Lab of Optic-Electronic and Communication, Jiangxi Sciences and Technology Normal University, Nanchang 330038, China*
[4]*School of Electromechanical Engineering, Guangdong University of Technology, Guangzhou 510006, Guangdong*
**jianzhang@gzhmu.edu.cn*

Abstract: Because of its similar genetic makeup with humans, zebrafish are an available and well-established osteoporosis model *in vivo* for anti-osteoporosis drug development as well as the drug safety-evaluation process. However, few optical imaging methods could effectively visualize the bone of adult zebrafish due to their limited penetration depth. In this paper, *in vivo* high-resolution and long-term characterization of a prednisolone-induced osteoporotic zebrafish model was achieved with spectral-domain optical coherence tomography (SD-OCT). The capability of three-dimensional SD-OCT imaging was also demonstrated in this study. With SD-OCT images, we could non-destructively monitor the deforming process of adult zebrafish skull from several directions at any time. There is good correlation and agreement between SD-OCT and histology. Valuable phenomenon such as bone defects could be quantitatively evaluated using the SD-OCT images at different time points during a period of 21 days.

1. Introduction

Osteoporosis is physiologic or pathologic loss of mineralized tissues resulting in metabolic disease, thus making it a chronic degenerative disease endangering the health of human. Reportedly by international osteoporosis foundation, there are more than 8.9 million fractures annually caused by osteoporosis, which implies every 3 seconds once osteoporosis fracture occurs [1–3]. When it comes to disease cause, aging, decreasing estrogen, and medical treatments such as glucocorticosteroids may play an important role [4–8]. On the basis of the fact that long-term treatment of glucocorticoid can induce osteoporosis, the animal models of osteoporosis can be successfully constructed [9,10]. For the highly similarity in the structure and genetics compared with human beings, zebrafish is an available and well-established osteoporosis model *in vivo* for studying bone deformations and dyspepsia [11–15]. A commonly used gold standard technique for assessing bone quality *in vitro*/*ex vivo* is histology [16,17]. However, histological sectioning and staining has insurmountable deficiency, mainly including all the animals have to be sacrificed, which will bring significant challenges in the study of biological procedures *in vivo*. In recent year, optical imaging techniques such as confocal microscopy, two photon microscopy and light sheet microscopy have become increasingly popular in biological study based on zebrafish. Undeniably, there

#353075 https://doi.org/10.1364/BOE.10.001184
Journal © 2019 Received 28 Nov 2018; revised 16 Jan 2019; accepted 27 Jan 2019; published 11 Feb 2019

Biomedical Optics EXPRESS

are many important biological processes revealed with the use of these imaging techniques. However, few of them can effectively detect the internal bone structure of the zebrafish after juvenile stages. Regarding the body size of adult zebrafish are far beyond the imaging depth of these imaging modalities, and zebrafish lose their transparency in the first two weeks of development, an appropriate optical imaging technique has to be used, which can achieve the high-resolution characterization of the adult zebrafish in the large field of view with good penetration depth and fast imaging speed.

Optical coherence tomography (OCT) is a robust and attractive imaging method that uses scattering light to reconstruct the three-dimensional images of biological tissues with a micrometer resolution [18,19], making OCT outstanding in the biological and biomedical imaging field [20–24]. Recently, the use of spectral-domain optical coherence tomography (SD-OCT) in zebrafish has been reported. In 2008, Larry Kagemann *et al.* confirmed the validity of OCT to monitor the development of eye, ear, heart, and spine based on an embryo 120 hours after fertilization [25]. In 2014, Ross F. Collery *et al.* explored the genetic, cellular, and signaling basis of emmetropization and myopia, as well as measured the axial length and other eye dimensions of zebrafish by SD-OCT [26]. Nevertheless, most of these works focused on early-stage zebrafish. Since 2016, we employed SD-OCT to study adult zebrafish. Our previous works demonstrated that SD-OCT can achieve *in vivo* three-dimensional characterization of the whole zebrafish brain [27]. Furthermore, the recovering process of a brain-injured adult zebrafish could be monitored with SD-OCT, which image quality can be comparable to pathology [28].

In this study, a SD-OCT system was employed for non-invasive characterizing the morphology of osteoporotic adult zebrafish model with high resolution. Long-terms *in vivo* imaging experiment, within a period of 21 days, was performed to demonstrate the deformation of the bone tissue.

2. Methods and materials

2.1 System design and imaging procedure

A SD-OCT imaging system (Fig. 1) was used in this study. The system was illuminated using a superluminescent diode (InPhenix, USA) with a central wavelength of 846.7 nm and bandwidth of 43.7 nm, resulting in a theoretical axial resolution of 7.24 μm in air. A 50/50 broad bandwidth spliced fiber coupler (Ziyin Photoelectric Technology, China) severs as the core of the interferometer. The spectrometer of this OCT system integrates a 1200 l/mm @ 840 nm volume phase holographic gratings (Wasatch Photonics, USA) and a 2048-pixel line-scan camera (SF-10-02K40-GE-02, Luster Co., Ltd., China). The line scan rate of the camera is 18 kHz in this study. The sample arm of the OCT system contains a pair of galvanometric scanners (Han's Motor, China) and a telecentric scan lens (achromat doublets, f = 40 mm, Daheng Optics, China). A custom C# language code was developed for operating the SD-OCT system. Another CCD camera was used to lively monitor the application area and take photographs of the samples. OCT imaging will be performed along a path that is selected based on the photograph of a sample.

Data acquisition and signal processing were performed using a high-performance personal computer. In this study, the scans were 3 × 3 mm and 2 mm in depth (300 × 300 × 500 pixels) centered on the head of zebrafish with a 18 kHz A-scan imaging speed. The acquisition time for a volumetric OCT image was ~7s. The volumetric image was generated from the 3D data sets with an open source software ImageJ 1.52a (National Institutes of Health, USA).

Biomedical Optics EXPRESS

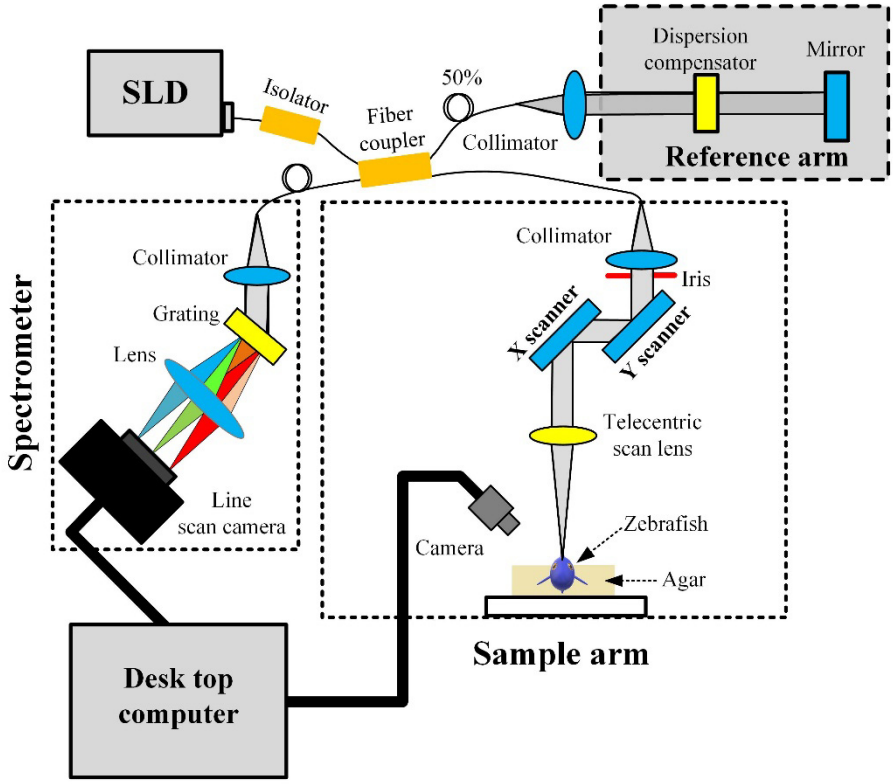

Fig. 1. SD-OCT imaging system used in this study.

2.2 Animal and ethics statement

The adult wild-type zebrafish were maintained in our flow-through aquaria at 28 ± 0.5 °C with a cycle of 14 h light and 10 h dark. Fish were fed two times daily with live brine shrimps and flake diet (Tetra, Melle). One third of the water volume (with or without prednisolone) was refreshed daily. *In vivo* experiments were performed in compliance with the guidelines on animal research stipulated by the Animal Care and Use Committee at Guangzhou Medical University.

2.3 Experimental protocols

Zebrafish (90 days old) were randomly assigned to three groups including control group (n = 10), 50 μM prednisolone-treatment group (n = 25), 125 μM prednisolone-treatment group (n = 25). All zebrafish were imaged with the OCT system at 0, 7, 14 and 21 days. For the *in vivo* experiment, the zebrafish were first anesthetized with 0.05% MS-222 in system water making them unresponsive to touch, after that agar gel were used to keep the their body up right. Furthermore, all zebrafish were imaged with OCT system at the suitable position, thus acquiring *in vivo* cross-sectional and sagittal-sectional OCT images. Immediately after OCT imaging, the zebrafish were return back to previous culture conditions for subsequent experiments. Finally all zebrafish were sacrificed 21 days later for histological analysis. During our experiment, ten zebrafish died naturally after 10 days post-induced. Furthermore, five zebrafish (82 days old) treated with 125 μM prednisolone were used to evaluate the capacity of 3D OCT imaging. After 7 days prednisolone treatment, the zebrafish received deep anesthesia to guarantee a high quality 3D image. All experimental protocols were shown in the Fig. 2.

Biomedical Optics EXPRESS

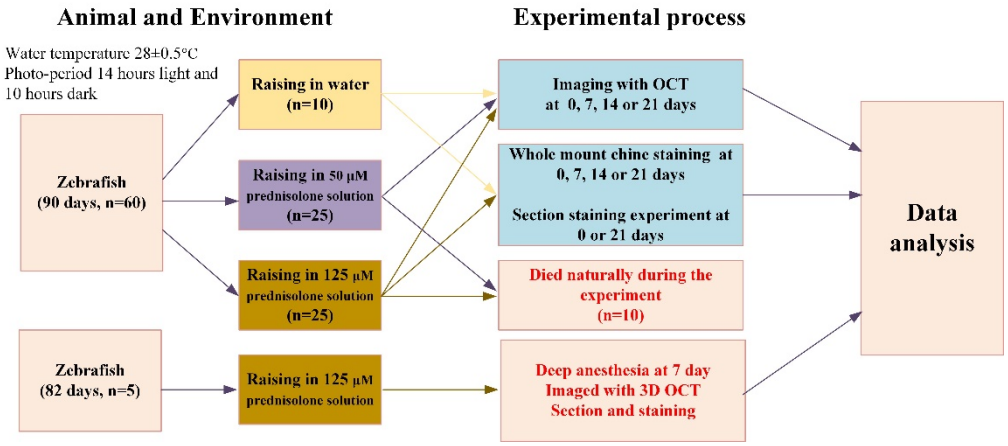

Fig. 2. The experimental protocols of this study.

2.4 Alizarin red staining

A commonly used technique for monitoring bone formation such as mineralised matrix deposition is alizarin red staining. On the basis of a dye which can attach specifically to calcium salts, alizarin red is widely used to observe and measure mineralisation of bone. Whole mount chine staining was performed as the following protocol [29]. After anesthesia, zebrafish were fixed with 4% parformaldehyde solution overnight, and soaked in 4% sodium chloride solution for 2 days, then the flesh were scraped away from the bones with tweezers. The whole bone were subjected to alizarin red staining (0.5% alizarin red, 0.7% KOH) on a shaker for 2 hours. After staining, samples were briefly washed 3 times with PBS Tween-20. The samples were placed in 100% glycerol for fixation. Finally, photographs were acquired digitally using a Leica stereo microscope (M125 C) under a 10 × objective. Section staining experiment was also performed as following protocol. After anesthesia, zebrafish were fixed with 4% paraformaldehyde solution for 12 hours, and then embedded inside paraffin. All samples were sectioned with a thickness of 8 μm and stained with 0.1% alizarin red. Finally, photomicrographs were taken using a digital pathology slide scanner (Leica CS2) with a 20 × objective and histomorphometric analysis.

3. Experimental results

3.1 System's resolution and imaging depth

Before *in vivo* experiment, we characterized the performance of the OCT system first. The axial resolution of the OCT system depends on the spectral characteristics of the light source. The spectrum of the superluminescent diode supplied by the manufacturer was shown in the Fig. 3(a), which central wavelength and bandwidth is 846.7 nm and 43.7 nm. The theoretical axial resolution of our OCT system is 7.24 μm in air that was calculated by the formula $R\_axial = (2\ln 2/\pi)*(\lambda^2/\Delta\lambda)$, where the λ is the central wavelength and the $\triangle\lambda$ is the spectral bandwidth. The lateral resolution of our OCT system was calculated by imaging a blade with sharp edges. Figure 3(b) gives the normalized amplitude of the OCT signal of a B-scan line across the blade edge, and corresponding edge-spread function was obtained. Taking the derivative of the edge-spread function yields the line-spread function [Fig. 3(c)], and the full width at half-maximum of the line-spread function quantifies the lateral resolution. The lateral resolution of our OCT system was ~12 μm. The phantom used for imaging-depth measurement was made by tilting a hair section into a 3% agar block. Figure 3(d) shows three OCT images of the phantom. The position of hair labeled with white dash arrows could be clearly found. The results demonstrated the imaging depth of our OCT system is up to 2 mm.

Biomedical Optics EXPRESS

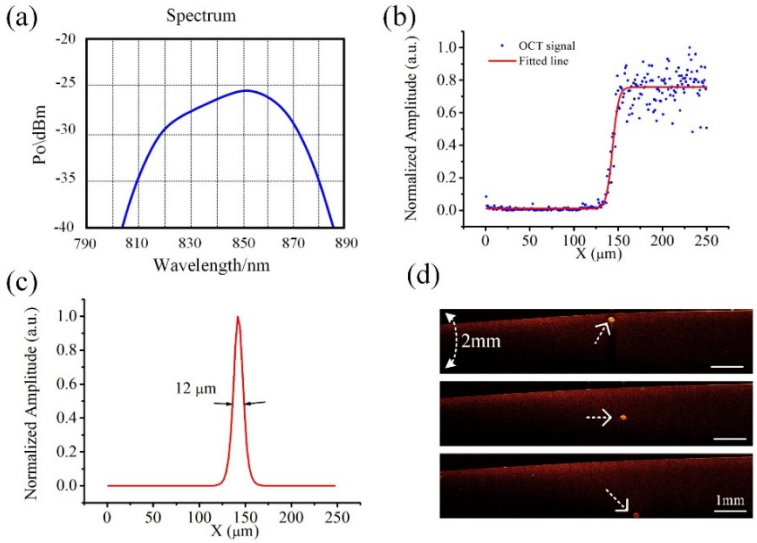

Fig. 3. (a) The spectrum of superluminescent diode used in the OCT system. (b) Normalized amplitude OCT signal of a B-scan line across a blade with sharp edges. (c) The lateral resolutions of the OCT imaging system. (d) OCT images of a hair section at different position.

3.2 Histological results

Zebrafish model was evaluated with whole mount chine alizarin red staining to give a comparison between the normal zebrafish (0 day) and osteoporotic zebrafish model (21 days). As shown in the Fig. 4(a), the alizarin red staining of chine from normal zebrafish presented symmetrical and bright. However, prednisolone-treated (125 μM, 21 days) zebrafish showed clearly decreased staining of the mineralized matrix, reflecting a decrease in bone mineral density and deterioration of trabecular bone. The optical density of zebrafish spine was measured with a professional pathological image analysis software Image-Pro plus 6.0 (Media Cybernetics, Inc., USA). As shown in the Fig. 4(b), the optical density of normal zebrafish was about two times high than that of zebrafish treated with prednisolone. These results demonstrated that adult zebrafish exhibit extensive osteoporosis after treated with prednisolone.

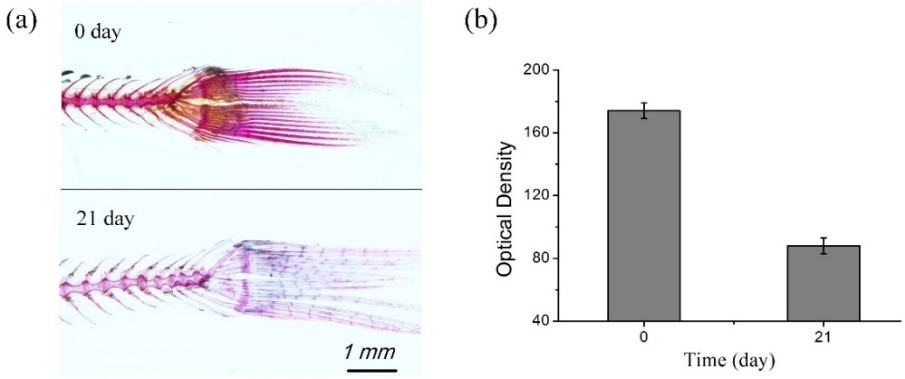

Fig. 4. Whole mount chine alizarin red staining results (a) and corresponding optical density (b) of normal zebrafish or zebrafish induced with 125 μM prednisolone 21 days.

Biomedical Optics EXPRESS

3.3 In vivo OCT imaging of prednisolone-induced osteoporosis

Zebrafish were *in vivo* image with OCT after anesthesia. The OCT images of normal zebrafish skull were given in the Fig. 5(a). Since the density of skull is higher than other tissues, that lead to more reflection when light passes through the skull. Thus, skull showed higher image intensity in the OCT images than other tissues labeled with green dash arrow. Based on the OCT image we could found that skull of normal adult zebrafish is smooth and symmetrical matched well with histological results as shown in the Fig. 5(b). After 21 days of prednisolone (125 μM) treatment, the region of low image intensity could be observed in the skull of zebrafish as shown in the Fig. 5(c) labeled with blue dash arrows. The low image intensity means the density of bone decrease at these area which named defect. The OCT imaging results was verified with histological results. *In vivo* OCT images can demonstrate the interruption of bone continuity after 21 days prednisolone-induction, revealing high consistency between OCT and histology.

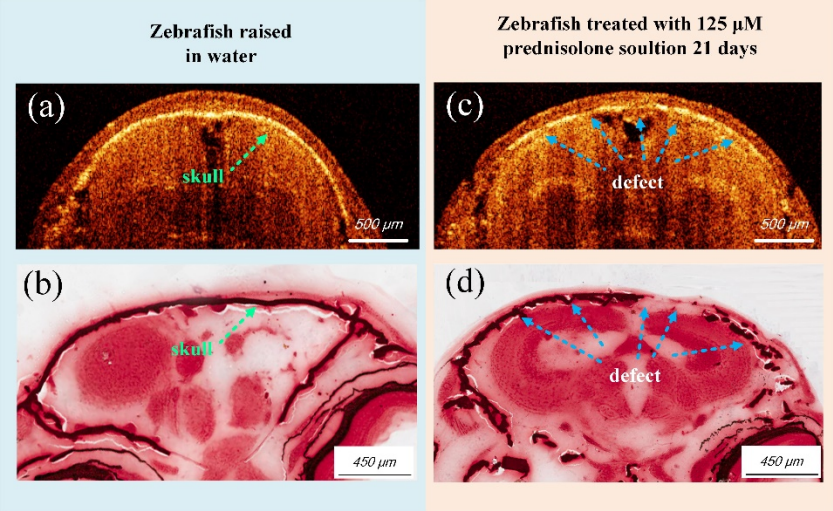

Fig. 5. (a) OCT image and histological result (b) of normal zebrafish skull. (c) OCT image and histological result (d) of skull of 21-days prednisolone (125 μM) induced zebrafish model.

Time-serial (0, 7, 14, or 21 days post-induced) *in vivo* OCT imaging was performed to give a visualized description of the osteoporotic process. All zebrafish were imaged twice at each time point using volume scan, first in the coronal plane and then in the sagittal plane. Cross-sectional OCT images of each zebrafish model showed osteoporotic feature were selected and used for analysis. Representative cross-sectional OCT image of osteoporotic zebrafish models at different time point was shown in the sagittal view [Fig. 6(a)] and the coronal view [Fig. 6(b)]. Zebrafish imaged at 0 day were healthy with their skull of high and uniform image intensity, suggesting that before drug-induction the skull was initially filled with bone trabeculae and marrow. With the progress of induction, bone defect gradually appeared, and 7 days later part of skull became low image intensity labeled with the dotted green rectangle, revealing the internal structure of their skull changed by prednisolone. The loss of bone calcium may explain lower imaging intensity of OCT images. Gradual loss of bone hard tissue in the zebrafish skull as the induction time lengthened, and regions of lower imaging intensity became more after 14 and 21 days. It is possible to clearly monitor the dynamic process of prednisolone-induced osteoporosis based on adult zebrafish model by OCT.

Biomedical Optics EXPRESS

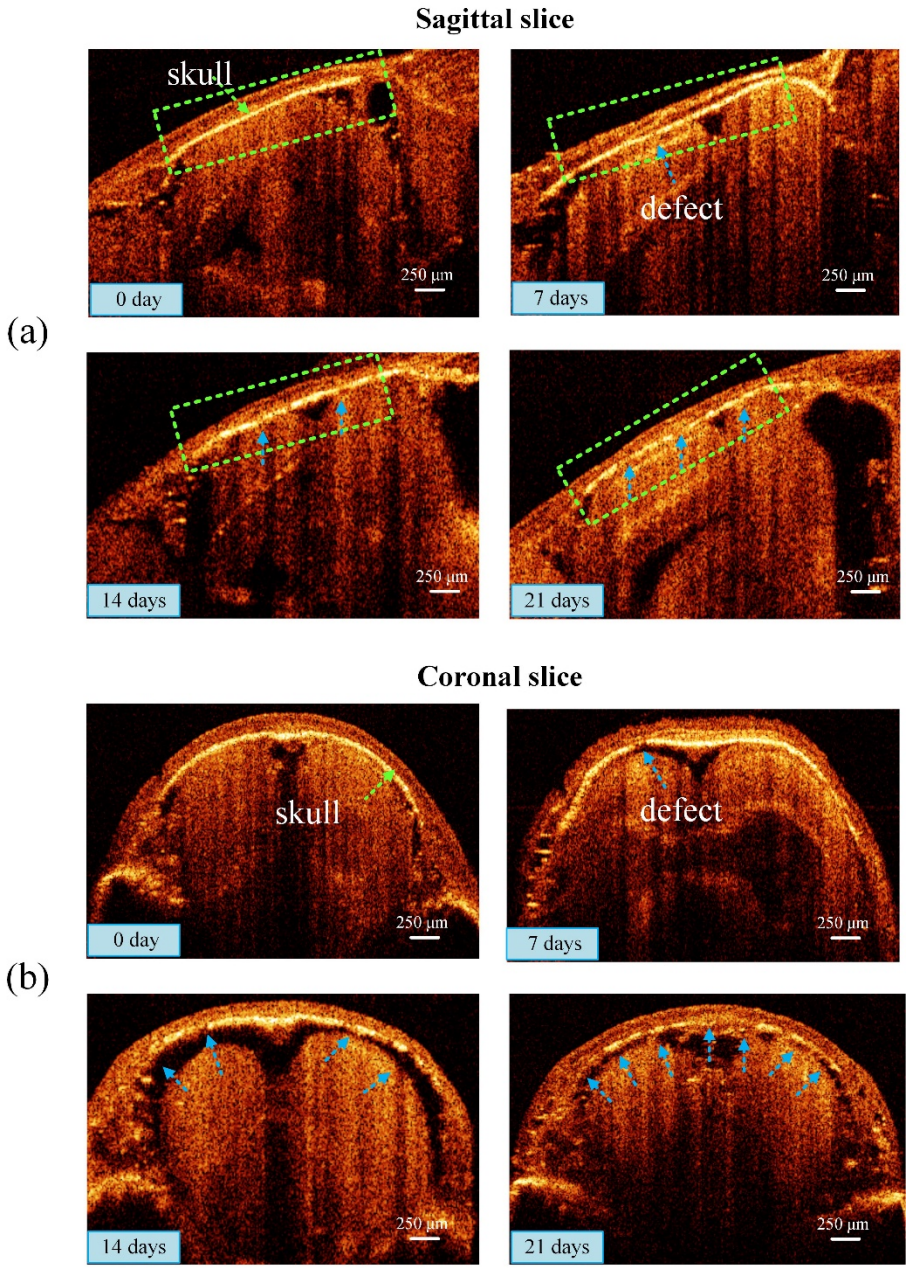

Fig. 6. The sagittal OCT images (a) and the coronal SD-OCT images (b) of adult zebrafish before (0 day) or after125 μM prednisolone treatment (7, 14 or 21 days).

Furthermore, OCT were employed to identify the severity of osteoporotic zebrafish model under different concentrations of prednisolone solution (50 or 125 μM). The OCT images of control group were also provided to exclude the possible effect such as the exposure of infrared light as shown in the Fig. 7(a). At 0 day, skull of both experimental group and control group featured a uniform and continuous structure. Bone defect evaluation is indispensable during osteoporosis image diagnosis. At 7 days, bone defects could be seen on OCT images of experimental group, while the skull of control group remained unchanged. At both 14 and 21 days, high concentration group had more bone defect regions than low concentration

Biomedical Optics EXPRESS

group. Obviously, the skull deformation is quicker and more serious in 125 μM prednisolone-treated group. Furthermore, a line chart based on the degree of skull rupture could be displayed as shown in the Fig. 7(b), which demonstrated a significant linear correlation existing between bone defect number with prednisolone concentration as well as the exposure time. Taken together, the OCT images indicated that long-term and high-doses of prednisolone will led to more serious osteoporosis.

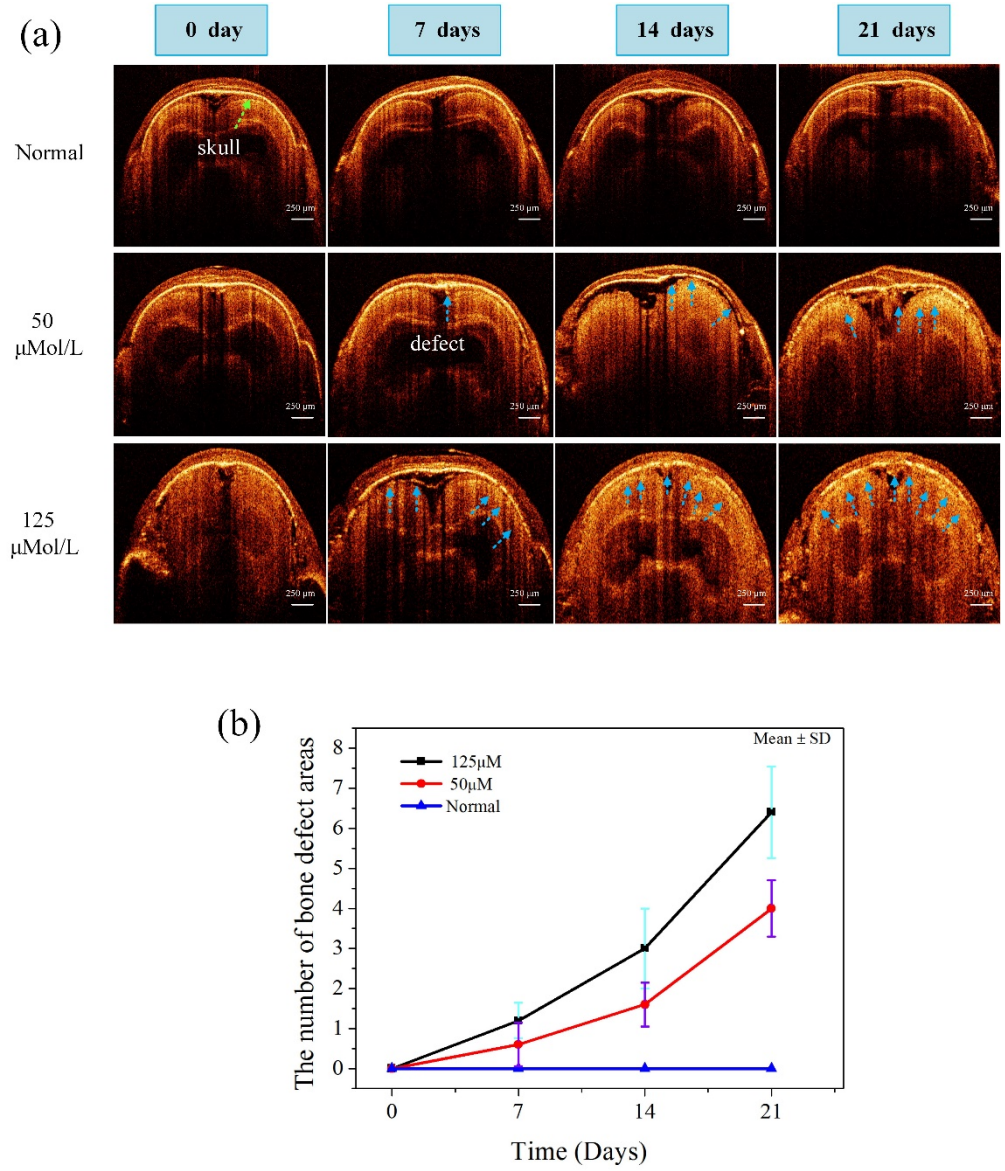

Fig. 7. (a) *In vivo* SD-OCT images of normal zebrafish and zebrafish treated with different concentrations of prednisolone (50 μM or 125 μM) at 0, 7, 14 or 21 days. (b) The defect number of skull *vs* exposure time and concentration of prednisolone.

3.4 Three-dimensional OCT imaging of prednisolone-induced osteoporosis

High resolution 3D imaging is an important advantage of OCT that was also assessed in this study. Figure 8(a) shows the 3D OCT image of a deep anesthetic zebrafish, which was treated

Biomedical Optics EXPRESS

with 125 μM prednisolone 7 days. Based on the 3D OCT image, continuous virtual slice was performed that could provide more accurate information about osteoporosis. Figure 8(b) was a sagittal images obtained from virtual slices that showed bone defect on the skull near the telencephalon of zebrafish labeled with green dash arrows. The further obtained coronal image [Fig. 8(c)] also demonstrated the skull near the telencephalon had bone defect. Figure 8(d) was the histological experiment result of the zebrafish obtained by coronal sectioning. Bone defect could be clearly identified on the skull near the telencephalon that confirm the accuracy of 3D OCT images.

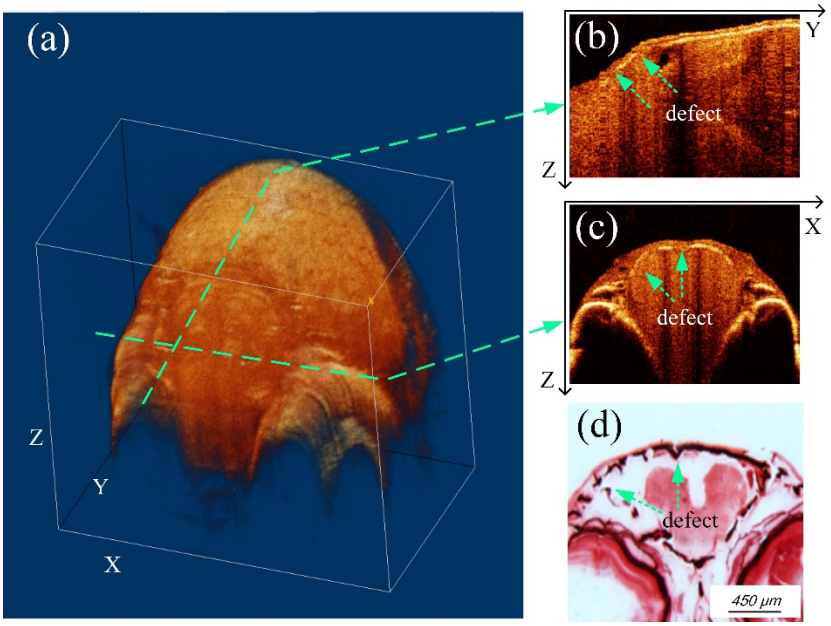

Fig. 8. (a) 3D OCT images of zebrafish head treated prednisolone (125 μM, 7 days). (b) and (c) is the sagittal images and the coronal image obtained from virtual slices along green dotted lines. (d) Corresponding histological image of the coronal image.

4. Discussions

Currently, zebrafish have become increasingly popular to model human diseases due to 87% similarity with human gene. The advantages of zebrafish model are rapid development, strong fecundity and low cost [14,15]. Another attractive feature of zebrafish is *in vitro* fertilization and embryos develop *in vitro*, and small size and good transparency in embryonic stage, making zebrafish propitious to model the dynamic process of diseases. It is so difficult in life sciences and with conventional techniques of image to monitor dynamic processes, thus *in vivo* imaging technologies arising. Although there are various imaging technologies aids for such detection, including confocal imaging, two photon microscopy and light-sheet microscopy [30–33], some problems still exist. Because there are various stages in the development of zebrafish, it is not easy to differentiate their structure properly, especially its adult stage. Obviously, studies based on zebrafish should not be confined to early stage. Degenerative diseases model, such as Alzheimer' disease and osteoporosis, should be constructed from adult or older zebrafish. Therefore, a high contrast technology with high imaging depth, high resolution and high imaging speed for adult zebrafish imaging is very important.

In general, given that a 30-day-old zebrafish can grow to 10 mm long, this is beyond the imaging depth of most optical imaging systems. It is well-known that 10 mm is the maximum depth of a commercial light-sheet microscope, which requires a transparent sample.

Biomedical Optics EXPRESS

Zebrafish, however, lose transparency in the first two weeks of development. For an adult zebrafish, its size is analogous to 30 × 10 × 5 mm cuboids, so that in order to image the adult zebrafish better, ultrasound imaging, magnetic resonance imaging and X-ray imaging have been applied. Wolfram Goessling *et al.* characterized liver tumors on zebrafish model with ultrasound biomicroscopy [34]. Eunseok Seo *et al.* achieved whole-body zebrafish imaging with the help of synchrotron X-Ray Micro-CT [35]. Samira Kabli *et al.* imaged the adult zebrafish with magnetic resonance microscopy that magnetic field intensity up to 9.4 Tesla [36]. Although conventional radiography is a popular imaging system, it uses ionizing X rays for imaging that has certain radiation hazard unavoidably. Magnetic resonance imaging can be another solution, but it also has a problem: slow and inconvenient imaging. At the same time, the swim bladder of zebrafish have much gas, which has adverse effects on ultrasound imaging. What's more, higher instrument costs also limit the application of these technologies.

Researches have demonstrated that zebrafish skull is absolutely suitable for studying bone growth and degradation [37,38]. These studies are based on pathological techniques to reveal the bone structure. Although conventional pathology are effective enough to distinguish the bone structure in most cases, irreversibly sample loss and cost might be made unnecessarily. In our previous studies, we successfully imaged the brain of adult zebrafish by SD-OCT. A long-rang SD-OCT system can provide three-dimensional image of the whole brain with a real time and non-invasive manner and achieve higher imaging depth [25]. For thorough study of both developmental biology and brain diseases, imaging subtler structure of the brain is essentially required.

In this study, the structures of adult zebrafish acquired with histology and OCT imaging system are compared and analyzed primarily to present an effective *in vivo* image mean that can monitor the development of osteoporosis with a real time, non-invasive and high-resolution manner. Long-term *in vivo* monitoring of prednisolone-induced osteoporosis on adult zebrafish was implemented from 0 to 21 days by using our SD-OCT system. The cross-sectional and sagittal-sectional SD-OCT images can provides the insight into the whole skull bone tissue, including morphology and functional structures. To the best of our knowledge, this is the first time that the prednisolone-induced osteoporosis of the adult zebrafish were *in vivo* characterized and evaluated with a SD-OCT imaging system.

Three-dimensional OCT imaging of osteoporotic adult zebrafish model was successfully achieved in this study. While this experiment exposed a problem in this study. Although we used anesthetics to keep the zebrafish from struggling, the zebrafish kept breathing throughout the scanning process. Due to a limited imaging speed, the problem of image dislocation is serious. Zebrafish had to receive deep anesthesia before the 3D OCT imaging experiment to guarantee a high quality 3D image. In the future, we will increase the scanning speed and use a displacement correction algorithm to solve this problem.

5. Conclusion

In this work we have demonstrated the feasibility of SD-OCT for *in vivo* monitoring and high-resolution characterizing the prednisolone-induced osteoporotic process on adult zebrafish. The image quality of SD-OCT is comparable to that of pathology. The unique imaging capability, security and convenience of SD-OCT enable it to be widely used in the study based on zebrafish.

Funding

National Natural Science Foundation of China (11704082, 11664011 and 81470724); Guangzhou Medical University; Guangzhou Science, Technology and Innovation Commission (201704030024); the Science and Technology Program of Jiangxi Province (20171ACB20027).

Biomedical Optics EXPRESS

Acknowledgments

Authors would like to thank Pro. Yonghong He (Graduate School of Tsinghua University at Shenzhen) and Dr. Qiang Huang (Shenzhen Sheng Qiang Technology Co., Ltd.) for their help in the development of SD-OCT imaging system.

Disclosures

The authors declare that there are no conflicts of interest related to this article.

References

1. K. Huo, S. I. Hashim, K. L. Yong, H. Su, and Q. M. Qu, "Impact and risk factors of post-stroke bone fracture," World J. Exp. Med. **6**(1), 1–8 (2016).
2. O. Ström, F. Borgström, J. A. Kanis, J. Compston, C. Cooper, E. V. McCloskey, and B. Jönsson, "Osteoporosis: burden, health care provision and opportunities in the EU," Arch. Osteoporos. **6**(1–2), 59–155 (2011).
3. J. Xu, M. Sun, Z. Wang, Q. Fu, M. Cao, Z. Zhu, C. Meng, Y. Yan, J. Mao, H. Tao, X. Huang, Z. Lin, T. Yang, and W. He, "Awareness of osteoporosis and its relationship with calcaneus quantitative ultrasound in a large Chinese community population," Clin. Interv. Aging **8**, 789–796 (2013).
4. H. Yin, S. Wang, Y. Zhang, M. Wu, J. Wang, and Y. Ma, "Zuogui Pill improves the dexamethasone-induced osteoporosis progression in zebrafish larvae," Biomed. Pharmacother. **97**, 995–999 (2018).
5. S. Pasqualetti, T. Congiu, G. Banfi, and M. Mariotti, "Alendronate rescued osteoporotic phenotype in a model of glucocorticoid-induced osteoporosis in adult zebrafish scale," Int. J. Exp. Pathol. **96**(1), 11–20 (2015).
6. L. A. Fitzpatrick, "Secondary causes of osteoporosis," Mayo Clin. Proc. **77**(5), 453–468 (2002).
7. B. L. Riggs, S. Khosla, and L. J. Melton 3rd, "A unitary model for involutional osteoporosis: estrogen deficiency causes both type I and type II osteoporosis in postmenopausal women and contributes to bone loss in aging men," J. Bone Miner. Res. **13**(5), 763–773 (1998).
8. K. Geurtzen, A. Vernet, A. Freidin, M. Rauner, L. C. Hofbauer, J. E. Schneider, M. Brand, and F. Knopf, "Immune suppressive and bone inhibitory effects of prednisolone in growing and regenerating zebrafish tissues," J. Bone Miner. Res. **32**(12), 2476–2488 (2017).
9. P. Moutsatsou, E. Kassi, and A. G. Papavassiliou, "Glucocorticoid receptor signaling in bone cells," Trends Mol. Med. **18**(6), 348–359 (2012).
10. R. S. Weinstein, "Glucocorticoid-induced bone disease," N. Engl. J. Med. **365**(1), 62–70 (2011).
11. P. Goldsmith, "Zebrafish as a pharmacological tool: the how, why and when," Curr. Opin. Pharmacol. **4**(5), 504–512 (2004).
12. S. Pasqualetti, G. Banfi, and M. Mariotti, "The zebrafish scale as model to study the bone mineralization process," J. Mol. Histol. **43**(5), 589–595 (2012).
13. G. Kari, U. Rodeck, and A. P. Dicker, "Zebrafish: an emerging model system for human disease and drug discovery," Clin. Pharmacol. Ther. **82**(1), 70–80 (2007).
14. G. J. Lieschke and P. D. Currie, "Animal models of human disease: zebrafish swim into view," Nat. Rev. Genet. **8**(5), 353–367 (2007).
15. L. I. Zon and R. T. Peterson, "In vivo drug discovery in the zebrafish," Nat. Rev. Drug Discov. **4**(1), 35–44 (2005).
16. J. L. Moore, M. Aros, K. G. Steudel, and K. C. Cheng, "Fixation and decalcification of adult zebrafish for histological, immunocytochemical, and genotypic analysis," Biotechniques **32**(2), 296–298 (2002).
17. J. M. Zodrow, J. J. Stegeman, and R. L. Tanguay, "Histological analysis of acute toxicity of 2,3,7,8-tetrachlorodibenzo-p-dioxin (TCDD) in zebrafish," Aquat. Toxicol. **66**(1), 25–38 (2004).
18. D. Huang, E. A. Swanson, C. P. Lin, J. S. Schuman, W. G. Stinson, W. Chang, M. R. Hee, T. Flotte, K. Gregory, C. A. Puliafito, and et, "Optical coherence tomography," Science **254**(5035), 1178–1181 (1991).
19. A. F. Fercher, "Optical coherence tomography," J. Biomed. Opt. **1**(2), 157–173 (1996).
20. K. Wang and Z. Ding, "Spectral calibration in spectral domain optical coherence tomography," Chin. Opt. Lett. **6**(12), 902–904 (2008).
21. G. Shi, Y. Dai, L. Wang, Z. Ding, X. Rao, and Y. Zhang, "Adaptive optics optical coherence tomography for retina imaging," Chin. Opt. Lett. **6**(6), 424–425 (2008).
22. P. Xi, K. Mei, T. Bräuler, C. Zhou, and Q. Ren, "Evaluation of spectrometric parameters in spectral-domain optical coherence tomography," Appl. Opt. **50**(3), 366–372 (2011).
23. Z. Zhan, X. Zhang, Q. Ye, and S. Xie, "Measurement of crater geometries after laser ablation of bone tissue with optical coherence tomography," Chin. Opt. Lett. **6**(12), 896–898 (2008).
24. Z. Wang, C. S. D. Lee, W. C. Waltzer, J. Liu, H. Xie, Z. Yuan, and Y. Pan, "In vivo bladder imaging with microelectromechanical-systems-based endoscopic spectral domain optical coherence tomography," J. Biomed. Opt. **12**(3), 034009 (2007).
25. L. Kagemann, H. Ishikawa, J. Zou, P. Charukamnoetkanok, G. Wollstein, K. A. Townsend, M. L. Gabriele, N. Bahary, X. Wei, J. G. Fujimoto, and J. S. Schuman, "Repeated, noninvasive, high resolution spectral domain optical coherence tomography imaging of zebrafish embryos," Mol. Vis. **14**, 2157–2170 (2008).

Biomedical Optics EXPRESS

26. R. F. Collery, K. N. Veth, A. M. Dubis, J. Carroll, and B. A. Link, "Rapid, accurate, and non-invasive measurement of zebrafish axial length and other eye dimensions using SD-OCT allows longitudinal analysis of myopia and emmetropization," PLoS One **9**(10), e110699 (2014).
27. J. Zhang, W. Ge, and Z. Yuan, "In vivo three-dimensional characterization of the adult zebrafish brain using a 1325 nm spectral-domain optical coherence tomography system with the 27 frame/s video rate," Biomed. Opt. Express **6**(10), 3932–3940 (2015).
28. J. Zhang, Z. W. Zhang, W. Ge, and Z. Yuan, "Long-term in vivo monitoring of injury induced brain regeneration of the adult zebrafish by using spectral domain optical coherence tomography," Chin. Opt. Lett. **14**(8), 081702 (2016).
29. W. Zhang, J. Xu, J. Qiu, C. Xing, X. Li, B. Leng, Y. Su, J. Lin, J. Lin, X. Mei, Y. Huang, Y. Pan, and Y. Xue, "Novel and rapid osteoporosis model established in zebrafish using high iron stress," Biochem. Biophys. Res. Commun. **496**(2), 654–660 (2018).
30. M. H. Malone, N. Sciaky, L. Stalheim, K. M. Hahn, E. Linney, and G. L. Johnson, "Laser-scanning velocimetry: a confocal microscopy method for quantitative measurement of cardiovascular performance in zebrafish embryos and larvae," BMC Biotechnol. **7**(1), 40 (2007).
31. Y. Z. Zhang, Y. C. Ouyang, Y. Hou, H. Schatten, D. Y. Chen, and Q. Y. Sun, "Mitochondrial behavior during oogenesis in zebrafish: a confocal microscopy analysis," Dev. Growth Differ. **50**(3), 189–201 (2008).
32. A. Kaufmann, M. Mickoleit, M. Weber, and J. Huisken, "Multilayer mounting enables long-term imaging of zebrafish development in a light sheet microscope," Development **139**(17), 3242–3247 (2012).
33. P. J. Keller, A. D. Schmidt, J. Wittbrodt, and E. H. Stelzer, "Reconstruction of zebrafish early embryonic development by scanned light sheet microscopy," Science **322**(5904), 1065–1069 (2008).
34. W. Goessling, T. E. North, and L. I. Zon, "Ultrasound biomicroscopy permits in vivo characterization of zebrafish liver tumors," Nat. Methods **4**(7), 551–553 (2007).
35. S. Kabli, A. Alia, H. P. Spaink, F. J. Verbeek, and H. J. De Groot, "Magnetic resonance microscopy of the adult zebrafish," Zebrafish **3**(4), 431–439 (2006).
36. K. M. Spoorendonk, C. L. Hammond, L. F. Huitema, J. Vanoevelen, and S. Schulte-Merker, "Zebrafish as a unique model system in bone research: the power of genetics and in vivo imaging," J. Appl. Ichthyology **26**(2), 219–224 (2010).
37. R. E. Mitchell, L. F. A. Huitema, R. E. H. Skinner, L. H. Brunt, C. Severn, S. Schulte-Merker, and C. L. Hammond, "New tools for studying osteoarthritis genetics in zebrafish," Osteoarthritis Cartilage **21**(2), 269–278 (2013).
38. S. C. Neuhauss, L. Solnica-Krezel, A. F. Schier, F. Zwartkruis, D. L. Stemple, J. Malicki, S. Abdelilah, D. Y. Stainier, and W. Driever, "Mutations affecting craniofacial development in zebrafish," Development **123**(1), 357–367 (1996).